ACS APPLIED MATERIALS & INTERFACES

Research Article

www.acsami.org

Carbon Nanotubes-Adsorbed Electrospun PA66 Nanofiber Bundles with Improved Conductivity and Robust Flexibility

Xiaoyang Guan,[†] Guoqiang Zheng,[*,†] Kun Dai,[†] Chuntai Liu,[†] Xingru Yan,[‡] Changyu Shen,[*,†] and Zhanhu Guo[*,‡]

[†]College of Materials Science and Engineering, The Key Laboratory of Material Processing and Mold of Ministry of Education, Zhengzhou University, Zhengzhou, P.R. China

[‡]Integrated Composites Laboratory (ICL), Department of Chemical & Biomolecular Engineering, University of Tennessee, Knoxville, Tennessee 37996, United States

Supporting Information

ABSTRACT: Electrospun polyamide (PA) 66 nanofiber bundles with high conductivity, improved strength, and robust flexibility were successfully manufactured through simply adsorbing multiwall carbon nanotubes (MWNTs) on the surface of electrospun PA66 nanofibers. The highest electrical conductivity (0.2 S/cm) and tensile strength (103.3 MPa) were achieved for the bundles immersed in the suspension with 0.05 wt % MWNTs, indicating the formation of conductive network from adsorbed MWNTs on the surface of PA66 nanofibers. The decrease of porosity for the bundles immersed in the MWNT dispersion and the formation of hydrogen bond between PA66 nanofibers and MWNTs suggest a superb interfacial interaction, which is responsible for the excellent mechanical properties of the nanocomposite bundles. Furthermore, the resistance fluctuation under bending is less than 3.6%, indicating a high flexibility of the nanocomposite bundles. The resistance of the nanocomposite bundle had a better linear dependence on the temperature applied between 30 and 150 °C. More importantly, such highest working temperature of 150 °C far exceeded that of other polymer-based temperature sensors previously reported. This suggests that such prepared MWNTs-adsorbed electrospun PA66 nanofiber bundles have great potentials in high temperature detectors.

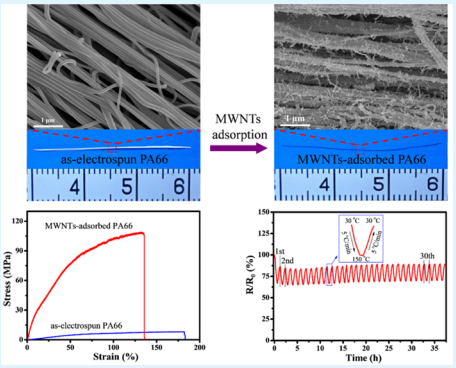

KEYWORDS: *electrospinning, carbon nanotube, nanocomposite bundles, conductive polymer composites, temperature detector*

1. INTRODUCTION

Electrospinning with its simplicity and versatility has produced fibers with diameter ranging from micrometers down to a few nanometers. These fibers have resulted in many promising applications in the fields of filtration, protective clothing, self-cleaning, drug delivery, electronic and photonic devices, etc.[1−4] Nowadays, electrospun fibers are generally collected in the form of nonwoven mats, and fibers in nonwoven mats are randomly arranged and nonuniform. Such a chaotic structure and relatively low mechanical strength have prohibited their applications. In order to solve the aforementioned problems, nanofiber bundles or yarns with macroscopic length have been elaborately fabricated recently.[5−8] Compared with the conventional nonwoven mat structure, the bundle shape endows the ultrafine electrospun fibers with many unique and promising advantages. For example, the aligned nanofiber bundles have demonstrated higher mechanical strength than randomly oriented nanofiber mats[9] and can be further woven into flexible textiles or integrated into clothes.[10,11] The macroscopical nanofiber bundles are desired for a wide range of applications, including tissue scaffolds,[12,13] reinforced composites,[14−16] and ultrasensitive sensors.[17,18]

Different methods have been proposed to obtain macroscopically nanofiber bundles.[19−24] For example, Wang and coworkers prepared high performed polyacrylonitrile (PAN) electrospun fiber yarns via a self-bundling electrospinning technique combined with postdraw and thermal treatment. After post-treatment, the electrospun PAN fiber yarn had a tensile strength of more than 370 MPa and a tensile modulus of more than 11 GPa.[24] In addition, various well-developed textile techniques, such as weaving, knitting, and braiding, were employed to process fibers into more complex three-dimensional (3D) fibrous structures to fine-tuned material properties. For example, Barber et al. fabricated braided nanofibrous scaffolds by braiding 3, 4, or 5 aligned bundles of electrospun poly(L-lactic acid) nanofibers, thus introducing an additional degree of flexibility to alter the mechanical properties of individual scaffolds.[25] On the premise of enhanced mechanical properties, the applications of electrospun polymer nanofiber bundles can be significantly expanded once they are endowed

Received: March 8, 2016
Accepted: May 12, 2016
Published: May 12, 2016

DOI: 10.1021/acsami.6b02888
ACS Appl. Mater. Interfaces 2016, 8, 14150−14159

with electrical property. Direct incorporating conductive guests into polymer matrix through solution casting,[26,27] melting processing,[28,29] or wetting spinning[30−32] is one of the easiest methods to prepare conductive polymer composites.

Carbon nanotube (CNTs) are known to exhibit superior structural, mechanical, chemical, electrical, and thermal performance.[33,34] CNTs are always directly added into electrospun solution to prepare ultrafine fiber composites with improved electrical conductivity.[35−37] However, the easy aggregation of CNTs in the nanofibers will deteriorate the nanofiber performance.[36,37] For example, Uddin et al.[37] dispersed CNTs into PAN polymer solution and produced nanocomposite yarns with a reduced tensile strength of about 40% due to poor CNT dispersion. An increased tensile strength of yarn by 35% was achieved by adding surfactant to obtain a better CNT dispersion. However, their electrical conductivity was still inferior because of the wrapping of CNTs with insulating polymers.[38,39] Thus, direct incorporating CNTs into polymer solution is not an effective way to fabricate electrical conductive electrospun fibers. Therefore, to prepare the electrospun ultrafine fibers with simultaneous improvements in mechanical property and electrical conductivity is still a challenge.

In this study, PA66 nanofiber bundles were first prepared by electrospinning and used as matrix materials to absorb conductive additive material of MWNTs. In this way, MWNTs absorbed on nanofiber surface could form a network, and therefore high electrical conductivity was introduced to the otherwise inert hosting PA66 nanofiber bundles. Meanwhile, higher tensile strength was observed in the MWNTs-adsorbed PA66 nanofiber bundles. The properties of the MWNTs-adsorbed PA66 nanofiber bundles were comparatively studied and the application potential to serve as temperature detector was evaluated 30−150 °C.

2. EXPERIMENTAL SECTION

2.1. Materials. Polyamide 6,6 (PA66), as a typical engineering thermoplastic material, was chosen for electrospinning to fabricate carbon nanotubes-adsorbed PA66 nanofiber bundles in this study arising from its good wear resistance and high mechanical strength or good stability under heating conditions. Meanwhile, PA66 nanofiber bundles have been successfully fabricated in our previous studies.[6,14] Moreover, it has been reported that the carboxylic CNTs can be adsorbed onto the electrospun polyamide nanofibers by hydrogen bonding.[38] PA66 (EPR-27) with a weight-average molecular weight of 2.0×10^4 g/mol was purchased from Shenma Group Co., Ltd., China. Carboxylic MWNTs with diameter between 20 and 30 nm, carboxyl content of 1.23 wt %, length of 30 μm, and purity over 95% were obtained from Chengdu Organic Chemicals Co. Ltd., Chinese Academy of Science. Formic acid (≥88%, analytical reagent) was purchased from Tianjin Chemical Reagents Plant. *N*,*N*-dimethylformamide (DMF, ≥ 99.5%, analytical reagent) was from Tianjin Fuyu Fine Chemical Co., Ltd., China. Deionized water was obtained from Dongguanshi nabaichuan water treatment equipment Co., Ltd. All the materials were used as received without any further purification.

2.2. Electrospinning. In order to obtain nanofiber bundles by electrospinning, a solution of PA66 (15 wt %) was prepared using formic acid (≥88%) as the solvent. The modified electrospinning apparatus (Figure 1a) consists of three components: a high voltage supplier (DW-N503−4ACCD, Tianjin Dongwen High Voltage Power Supply Plant); a spinneret with a diameter of 0.5 mm; two electrode pins with a diameter of 0.5 mm serving as collector. The distance between the two pins was 3 cm. Electrospinning was carried out at an applied voltage of 25 kV over a distance of 25 cm from spinneret to collector. Environmental temperature and relative humidity were 25 ± 2 °C and 45 ± 5%, respectively. All other surrounding metallic sources were shielded from the high voltage components during electrospinning.

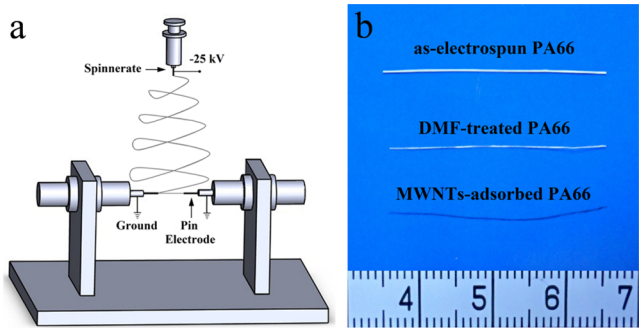

Figure 1. (a) Schematic of the modified electrospinning setup used to fabricate PA66 nanofiber bundle and (b) digital photo of as-electrospun PA66, DMF-treated PA66, and MWNTs-adsorbed PA66 (immersed in 0.05 wt % MWNT dispersion).

2.3. Preparation of MWNT Dispersion. Different quantities of MWNTs were dispersed in DMF to obtain MWNT dispersions with various concentrations (0.03, 0.05, 0.1, 0.2, 0.5 wt %). Ultrasonication was then applied to the MWNT dispersion for 1 h at 0 °C using a Scientz-IID Ultrasonic Homogenizer (Ningbo Scientz Biotechnology Co., China) with a nominal frequency of 20 kHz and a power of 285 W.

2.4. Adsorption of MWNTs on PA66 Nanofibers in Bundles. The electrospun PA66 nanofiber bundles (as-electrospun PA66) were immersed in a glass bath containing the MWNT dispersion and subjected to ultrasonication with a sonication wand. The power and frequency for the ultrasonication were 285 W and 20 kHz. Various adsorption time was performed (1, 5, 10, 20, 30, and 60 min) to determine different MWNT contents in the MWNTs-adsorbed PA66 nanofiber bundles (MWNTs-adsorbed PA66). Therefore, the relationships between the electrical, mechanical properties, and adsorption time were obtained. The MWNTs-adsorbed PA66 were rinsed briefly in deionized water for several times in order to remove the residuals and DMF solvent on the bundle surface. Finally, the MWNTs-adsorbed PA66 were dried at 60 °C in a vacuum oven for 24 h. The MWNTs-adsorbed PA66 with the adsorption time of 10 min showed the optimal electrical and mechanical property (see Figures S1 and S2 in the Supporting Information). For comparison, the electrospun PA66 nanofiber bundles treated with pure DMF (DMF-treated PA66) were also prepared.

2.5. Thermogravimetric Analysis. Thermogravimetric analysis was performed under a nitrogen atmosphere on a TGA/TA Q50 (TA Instruments Co., U.S.A.) from 30 to 600 °C with a heating rate of 20 °C/min to determine the MWNT content in MWNTs-adsorbed PA66. To ensure the accuracy of the result, at least 3 specimens were tested for each sample.

2.6. Electrically Conductive Property Test. For conductive property test, the electrical resistances were measured by a high resistivity meter (model TH2683, Changzhou Tonghui Electronics Co., Ltd.) and a digital multimeter (FUKE-DT9205, Shenzhen Fuke Instrument Co., Ltd.). Two carbon fiber wires served as electrodes to connect the composite bundles using conductive silver paste. The distance between two electrodes was 10 mm. To ensure the accuracy of the result, at least 6 specimens were tested for each experiment condition.

2.7. Mechanical Property Test. For mechanical measurements, the specimens were stabilized on a self-made paper frame with the gage length of 10 mm (see Figure S3) and tested on a universal tensile testing machine (UTM2203, Sun Technology Stock Co., Ltd.) equipped with a 100 N load cell at a crosshead rate of 0.1 mm/min. For each condition, the average value reported was derived from at least 6 tested specimens. An Olympus BX51 optical microscope was used to determine the bundle diameter required for mechanical and electrical measurements.

DOI: 10.1021/acsami.6b02888
ACS Appl. Mater. Interfaces 2016, 8, 14150−14159

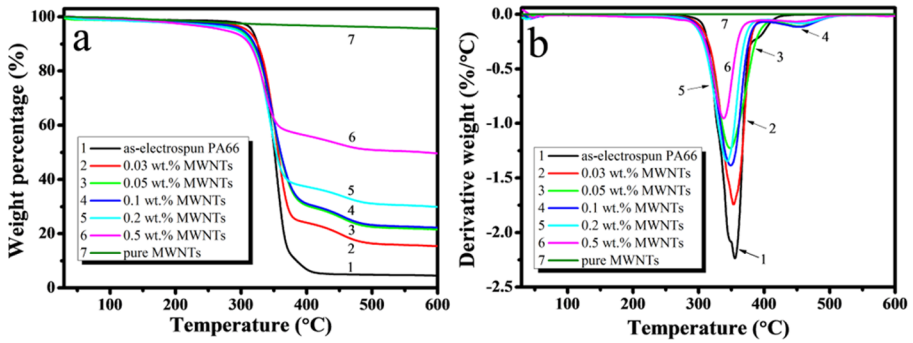

Figure 2. (a) TGA curves and (b) DTG curves of pure MWNTs, as-electrospun PA66 and MWNTs-adsorbed PA66 prepared with different concentrations of MWNT dispersion.

Table 1. TGA Results of Nanocomposite Bundles Prepared with Different Concentrations of MWNT Dispersion

samples	T_{onset}(°C)	T_{max}(°C)	residue (wt %)	ω_{MWNTs}(wt %)
as-electrospun PA66	334	355	4.51	0
0.03 wt % MWNTs	330	353	15.38	10.87
0.05 wt % MWNTs	324	350	21.57	17.06
0.1 wt % MWNTs	320	348	23.48	17.76
0.2 wt % MWNTs	318	343	29.85	25.34
0.5 wt % MWNTs	309	333	49.58	45.07

2.8. SEM Observation. The morphology and tensile fracture surface of as-electrospun PA66, DMF-treated PA66, and MWNTs-adsorbed PA66 were observed by scanning electron microscope (JEOL JSM 7500F) operated with an accelerated voltage of 5 kV. Before observation, the specimens were sputtered with a thin layer of gold for better imaging.

2.9. FT−IR. Fourier transform infrared spectroscopy (FT−IR) measurements were conducted on a Nicolet iS50 instrument with the attenuated total reflection (ATR) mode. All the spectra were obtained in the range from 500 to 4000 cm^{-1} at a resolution of 4 cm^{-1}.

2.10. Flexibility Test. The resistance changes of MWNTs-adsorbed PA66 under different bending angles (0°, 45°, 90°, 135°, 180°) and bending for 1000 consecutive cycles with a bending angle of 180° were measured by a digital multimeter (FUKE-DT9205, Shenzhen Fuke Instrument Co., Ltd.). For each condition, 5 different samples with length of 3 cm were taken, and the representative data were reported.

2.11. Temperature-Resistance Test. Before temperature-resistance test, the electrical conductivity of MWNTs-adsorbed PA66 at different temperatures was investigated in terms of current−voltage ($I-V$) measurement. Then, the temperature-resistance test was conducted on a Linkam THMS 600 hot-stage having the capability to precisely control the temperature, and the resistance of MWNTs-adsorbed PA66 versus temperature was recorded by a computer equipped with a high resistivity meter (model TH2683, supplied by Changzhou Tonghui Electronics Co., Ltd.). The specimen length was 10 mm. The resistance data were obtained simultaneously as a function of the applied temperature. In order to investigate the temperature sensing performance of MWNTs-adsorbed PA66, measurements with different temperature protocols were conducted. First, the resistance change of MWNTs-adsorbed PA66 over a wide temperature range from 30 to 270 °C at 5 °C/min was studied. According to this result combined with the DSC curve (see Figure S4), it was found that the nanocomposite bundle was not melt yet at 150 °C, and moreover the resistance could vary with the temperature below 150 °C in a linear manner. Then, the protocols followed were 33 consecutive heating/cooling cycles between 30 and 150 °C. At the beginning of each cycle, the temperature was maintained constant at 30 °C for 10 min for the purpose of temperature stabilization. Then, the specimen was heated from 30 to 150 °C at 5 °C/min, held at this temperature for 10 min, and then cooled down to 30 °C at the same rate.

3. RESULTS AND DISCUSSION

3.1. Electrical Conductive Property. The macroscopically electrospun PA66 nanofiber bundles (i.e., as-electrospun PA66), bundles treated in DMF (i.e., DMF-treated PA66), and MWNTs dispersions (i.e., MWNTs-adsorbed PA66), with a length of approximately 3 cm, were successfully prepared (see Figure 1b). The diameter of as-electrospun PA66 is in the range of 100 to 120 μm. Compared with as-electrospun PA66, the diameter of DMF-treated PA66 and MWNTs-adsorbed PA66 (immersed in 0.05 wt % MWNT dispersion) was significantly decreased.

TGA was performed on MWNTs-adsorbed PA66 prepared using MWNT dispersion with various MWNT concentrations, as well as on as-electrospun PA66 and pure MWNTs, to examine the amount of MWNTs adsorbed on the PA66 nanofiber surface and to evaluate the thermal stability of these samples. Figure 2a shows the TGA curves of the samples, and Figure 2b shows the corresponding derivative thermogravimetric (DTG). Table 1 shows the temperature, at which the samples begin to decompose (T_{onset}), the temperature at which the maximum DTG occurs (T_{max}), the percentage of residue between 550 and 600 °C, and the content of MWNTs in MWNTs-adsorbed PA66. The content of MWNTs in the composite nanofiber bundles was estimated using Equation 1:

$$\omega_{MWNTs} = C_C - C_A \quad (1)$$

where C_C is the weight loss percentage of MWNTs-adsorbed PA66, C_A is the weight loss percentage of as-electrospun PA66, and ω_{MWNTs} is the content of MWNTs in MWNTs-adsorbed PA66. As can be seen in Figure 2a, the mass loss of MWNTs is as low as 4.42 wt % at 600 °C. All the MWNTs-adsorbed PA66 degrades in a similar manner to that of as-electrospun PA66, indicating that MWNT adsorption can not essentially change the thermal properties of PA66 nanofiber bundles. Furthermore, as shown in Figure 2b and Table 1, as-electrospun PA66 begins to degrade at approximately 340 °C and the major decomposition region around 340−430 °C should be attributed to the degradation of PA66 (black line in Figure 2a, b).

DOI: 10.1021/acsami.6b02888
ACS Appl. Mater. Interfaces 2016, 8, 14150−14159

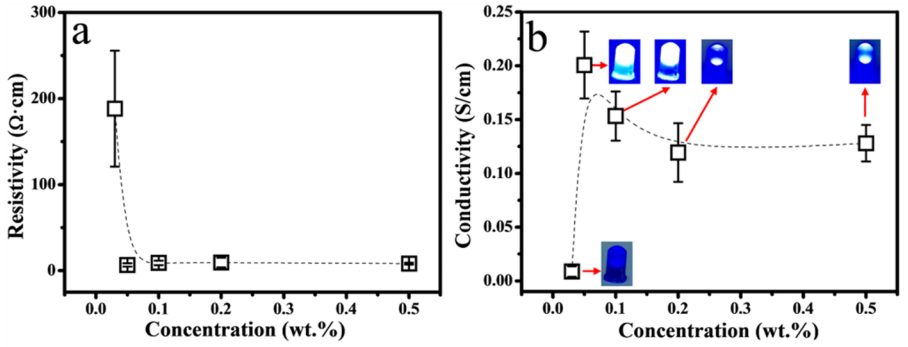

Figure 3. Dependence of the (a) resistivity and (b) conductivity on the concentration of MWNT dispersion. Inset images in (b) are the photographs of LED with different lightness.

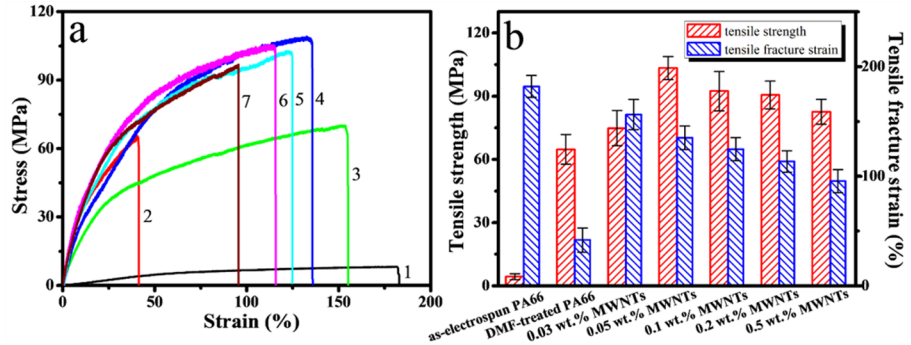

Figure 4. (a) Typical stress−strain curves of (1) as-electrospun, (2) DMF-treated, and MWNTs-adsorbed PA66 bundles from MWNTs concentrations of (3) 0.03 wt %, (4) 0.05 wt %, (5) 0.1 wt %, (6) 0.2 wt %, and (7) 0.5 wt % and (b) dependence of the tensile strength and tensile fracture strain on the concentration of MWNT dispersion.

However, the addition of MWNTs accelerates the degradation of MWNTs-adsorbed PA66. Moreover, it is noted that T_{onset} and T_{max} for MWNTs-adsorbed PA66 generally shift toward lower temperature with increasing the concentration of MWNT dispersion. In other words, MWNTs adsorbed on the surface of PA66 nanofiber serve as catalyst to rapidly degrade the electrospun PA66 nanofibers, which has been reported in the electrospun nylon-6,6 nanofibers.[40] Considering that MWNT has higher thermal stability,[40] this result is somewhat interesting and the possible explanation for this can be understood as follows. On one hand, MWNT has a very high thermal conductivity up to 3000 W/mK,[41] thus the heat can be efficiently transferred into the inner layer of nanocomposite bundle and the degradation of inner PA66 fibers is effectively accelerated. On the other hand, the possible trace water in MWNTs can accelerate the hydrolysis of PA66, resulting in a faster decomposition of MWNTs-adsorbed PA66.[41] Moreover, the nanocomposite bundles prepared with higher MWNT dispersion concentration generally show a higher content of MWNTs (see Figure 2a and Table 1).

The electrical property of MWNTs-adsorbed PA66 prepared with different concentrations of MWNT dispersion was carefully investigated, and the representative data are listed in Figure 3. The resistivity of MWNTs-adsorbed PA66 is observed to generally decrease with increasing the concentration of MWNT dispersion, Figure 3a. As for the conductivity of composite nanofiber bundles (see Figure 3b), it increases sharply in lower concentration range (less than 0.1 wt %) with increasing the concentration of MWNT dispersion, meaning that the MWNT dispersion with lower concentration can significantly improve the conductivity. The conductivity increases to a maximum of 0.2 S/cm when the concentration of MWNT dispersion is 0.05 wt %. Unexpectedly, with further increase in the concentration, the average conductivity decreases slightly and then generally keeps constant in higher concentration range. These indicate that ideal network of MWNTs at the surface of PA66 nanofibers can be developed at lower concentration of 0.05 wt %, whereas the higher MWNT content can not offer remarkable contribution to the improvement of conductivity. Furthermore, using MWNTs-adsorbed PA66 bundles, we constructed a simple circuit to power a light-emitting diode (LED), photographs of the LED with different lightness are observed (see the insets in Figure 3b). Obviously, with increasing the MWNTs concentration, the trend of LED lightness level is consistent with the conductivity.

3.2. Mechanical Properties. To investigate the influence of MWNT concentration in dispersion on the mechanical properties of MWNTs-adsorbed PA66, a series of monotonic tensile tests were carried out. Figure 4a shows the typical stress−strain curves of as-electrospun PA66, DMF-treated PA66, and MWNTs-adsorbed PA66 prepared with different concentrations of MWNT dispersion. On the whole, it is found that all the stress−strain curves of composite nanofiber bundles exhibit similar shape. The tensile strength and tensile fracture strain of samples can be recorded from the stress−strain curves and their dependence on the concentration of MWNT dispersion is shown in Figure 4b. Clearly, the tensile strength of MWNTs-adsorbed PA66 prepared with 0.05 wt % MWNT dispersion has been increased by up to 2380% compared with that of as-electrospun PA66 and by up to 60% compared with DMF-treated PA66. It should be noted that DMF-treated PA66 shows a much higher tensile strength than as-electrospun PA66

DOI: 10.1021/acsami.6b02888
ACS Appl. Mater. Interfaces 2016, 8, 14150−14159

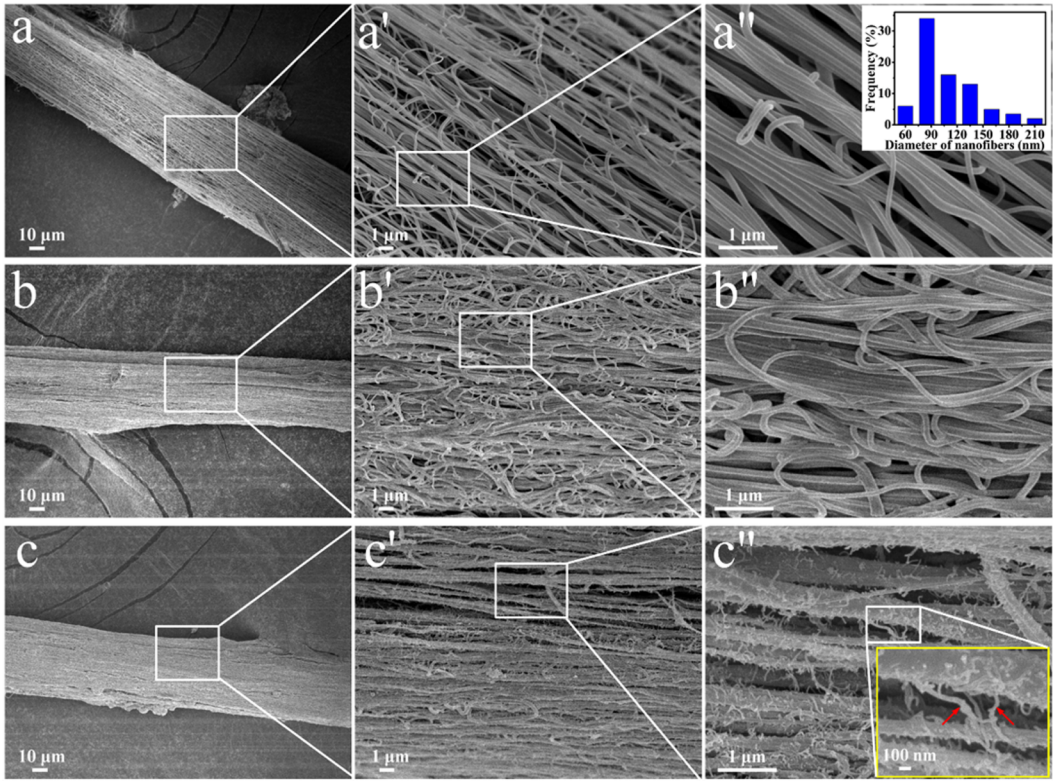

Figure 5. Morphology of (a–a″) as-electrospun PA66, (b–b″) DMF-treated PA66, and (c–c″) MWNTs (0.05 wt % MWNT)-adsorbed PA66 at different magnifications. The inset image in (a″) is the diameter distribution of PA66 nanofibers and the inset in (c″) is a higher magnification image. The red arrows show MWNTs adsorbed on the nanofiber.

because the bundle shrinks (see Figure 1b) and the interaction among PA66 nanofibers is increased after the DMF treatment.[14] Figure 4b also shows that the tensile strength of MWNTs-adsorbed PA66 first increases and then decreases with increasing the concentration of MWNT dispersion. Obviously, the critical concentration point appears to be 0.05 wt %. As previously reported,[42] MWNTs decorated on the surface of electrospun nanofiber will decrease the slippage of nanofibers by interconnecting them. Reasonably, an appropriately higher amount of MWNTs will improve the interconnecting function and results in a higher tensile strength. However, with further increasing the MWNT concentration beyond the critical concentration, more MWNTs will aggregate and hinder the effective adsorption of MWNTs. As a result, the tensile strength of nanocomposite bundles gradually decreases with further increasing the concentration of MWNT dispersion. The recorded tensile fracture strain of MWNTs-adsorbed PA66 composites declines slightly with increasing the concentration of MWNT dispersion (see Figure 4b). However, compared with as-electrospun PA66, no significant decrease in the tensile fracture strain is observed in MWNTs-adsorbed PA66 (see Figure 4b), indicating that such nanocomposite bundles still show a certain degree of toughness.

As can be seen from Figures 3 and 4, both electrical conductivity and tensile strength of the MWNTs-adsorbed PA66 simultaneously reach the maximum values when the concentration of MWNT dispersion is 0.05 wt %. In other words, the high conductivity and tensile strength, viz., balanced electrical, and mechanical properties of such nanocomposite bundles can be achieved when the concentration of MWNT dispersion is 0.05 wt %. Therefore, in the following section, only the nanocomposite bundles prepared with 0.05 wt % MWNT dispersion were investigated. Furthermore, the influence of adsorption time of MWNTs on electrical and mechanical properties was also studied. As shown in Figures S1 and S2, the optimum adsorption time was found to be 10 min. Therefore, an adsorption time of 10 min was chosen to fabricate MWNTs-adsorbed PA66 with high performance in the following section.

3.3. Morphology. To better understand the high electrical and mechanical properties of MWNTs-adsorbed PA66, the surface morphologies of as-electrospun PA66, DMF-treated PA66, and MWNTs-adsorbed PA66 were observed by SEM Figure 5a–a″ shows the typical SEM images of as-electrospun PA66. The bundle diameter is observed uniform locally and most nanofibers align along the bundle's longitudinal axis apart from a small amount of randomly arranged ones, Figure 5a. The inset image in Figure 5a″ displays the diameter distribution of electrospun PA66 fibers. Obviously, the diameter of these fibers is in the range of 60–230 nm, and the mean diameter is about 110 nm, indicating that the diameter is indeed at nanoscale.[7,43] Under a higher magnification (see Figure 5a′, a″), as-electrospun PA66 nanofibers are observed to have very smooth surface with many pores and gaps between the nanofibers. Compared with as-electrospun PA66, the diameter of DMF-treated PA66 and MWNTs-adsorbed PA66 is observed to be significantly decreased (see Figure 5a–c), consistent with the optical photograph (see Figure 1b). Furthermore, as shown in Figure 5b′, b″, the porosity (viz., voids between nanofibers) of DMF-treated PA66 is smaller than that of as-electrospun PA66. The explanation can be understood as follows: PA66 nanofibers are easier to infiltrate in the polar solvents like DMF, thus the nanofibers tend to stick together once DMF is evaporated, and a decreased porosity is

DOI: 10.1021/acsami.6b02888
ACS Appl. Mater. Interfaces 2016, 8, 14150–14159

expected. After the incorporation of the MWNTs by ultrasonication, the diameter of the resultant MWNTs-adsorbed PA66 further decreases compared with as-electrospun PA66. In addition, the distance between nanofibers obviously decreases, as confirmed by high-magnification SEM pictures (see Figure 5c′, c″). The surface of PA66 nanofibers becomes very rough after the adsorption of MWNTs (see Figure 5c″). That is, many MWNTs are densely adsorbed on the nanofibers, as confirmed by the inset image in Figure 5c″. Some MWNTs are observed protruding from one nanofiber, connecting with other nanofibers. It is worth noting that the pores in electrospun PA66 nanofiber bundle are not covered by MWNTs, making it possible to take advantage of the large number of interconnected pores in the electrospun nanofiber bundles. Moreover, MWNTs are observed to enter the interior of nanocomposite bundles and are adsorbed on the surface of interior nanofibers. Such adsorption must be strong since MWNTs remain on the surface even after washing in deionized water for several times, implying that MWNTs are not simply located on the nanofiber surface. Instead, they are strongly adhered to the PA66 nanofibers via hydrogen bond. The reason is as follows: a hydrogen bond is expected between amide groups (—NHCO—) from PA66 and the carboxylic groups (—COOH) from the carboxylic MWNTs.[38,44] Therefore, high tensile strength of MWNTs-adsorbed PA66 can be ascribed to the combined action of MWNTs and DMF. On the one hand, a better wettability between DMF and PA66 nanofibers allows MWNTs to easily adsorb on the nanofibers (Figure 5a″ and c″), drawing nanofibers closer. On the other hand, the hydrogen bond between the nanofibers and carboxylic MWNTs improves the stress transfer efficiency and thereby enhances the tensile strength of MWNTs-adsorbed PA66.

The chemical interaction between MWNTs and PA66 nanofibers after the adsorption process can be revealed by FT−IR test, Figure 6. Compared with as-electrospun PA66, no

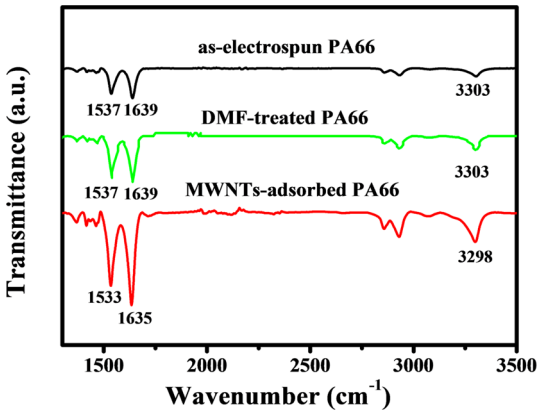

Figure 6. FT−IR spectra of as-electrospun PA66, DMF-treated PA66, and MWNTs-adsorbed PA66 (immersed in 0.05 wt % MWNT dispersion).

obvious peak shifts are observed after DMF treatment. However, several peaks for PA66 nanofiber are observed to have shifted after the MWNT adsorption. For example, the peak at 1537 cm^{-1}, belonging to the adsorption peak of amide (II), shifts to 1533 cm^{-1}. The adsorption peak of amide (I) slightly changes from 1639 to 1635 cm^{-1}. In addition, the adsorption peak of amine group at 3303 cm^{-1} shifts to 3298 cm^{-1}. Such changes suggest the chemical interactions between PA66 macromolecular chain and MWNTs.[42,45] The interfacial interaction between PA66 and MWNTs is another factor beneficial to the reinforcement of the MWNTs-adsorbed PA66 nanofiber bundles.

To better understand the role of interfacial interaction between the PA66 nanofibers and MWNTs on mechanical properties, the tensile fracture surfaces of as-electropun PA66, DMF-treated PA66, and MWNTs-adsorbed PA66 are presented. Figure 7a−a″ shows the tensile fracture surface of as-electrospun PA66. It can be seen that as-electrospun PA66 is necked (see Figure 7a) after fracture and numerous PA66 nanofibers are pulled out from the bundle. Moreover, these drawn nanofibers are seriously tortuous (see Figure 7a″). This suggests that as-electrospun PA66 exhibits the typical ductile fracture characteristic, which coincides well with the stress−strain curve, Figure 4a. With respect to DMF-treated PA66 (see Figure 7b−b″), its fractured surface is relatively flush, viz., obvious necking can not be found in the fractured region. Additionally, the PA66 nanofibers in bundle tend to be directly broken instead of being pulled out from the bundle. This well explains the observed significantly enhanced tensile strength of DMF-treated PA66 compared with as-electrospun PA66. For MWNTs-adsorbed PA66, its fractured surface is evener than that of DMF-treated PA66 (see Figure 7c). Interestingly, many PA66 nanofibers are still protruded out from the tip of fractured surface (see Figure 7c′, c″), and moreover they are sinuous and exhibit large deformation. Combined with the fractured behavior of DMF-treated PA66, the protruded and sinuous nanofibers (shown in Figure 7c′, c″) imply that the adsorption of MWNTs can endow composite bundle with toughness. More importantly, the inset in Figure 7c″ shows that MWNTs (as indicated by the red arrows) are still adsorbed on the surface of PA66 nanofibers after fracture, suggesting the superb interfacial interaction between PA66 nanofibers and MWNTs. This is also consistent with the FT-IR result shown in Figure 6. Therefore, the enhanced mechanical properties of MWNTs-adsorbed PA66 (immersed in 0.05 wt % MWNTs dispersion) can be ascribed to the decrease of porosity for the bundles as well as the superb interfacial interaction between PA66 nanofibers and MWNTs.

3.4. Flexibility. The MWNTs-adsorbed PA66 nanocomposite bundles also exhibit a good flexibility. Because the MWNTs-adsorbed PA66 prepared with 0.05 wt % MWNT concentration exhibits the highest conductivity, tensile strength, and good toughness (see Figures 3 and 4), it is chosen for flexibility characterization. The relative resistance change of MWNTs-adsorbed PA66 composite nanofiber bundles under different bending angles and bending for 1000 consecutive cycles with a bending angle of 180° is respectively shown in Figure 8a, b. R_0 and R correspond to the resistance before and after bending, respectively. The recorded resistance value is normalized by the samples initial resistance value R_0 (viz., R/R_0). As can be seen, the resistance fluctuation is less than 3.6% under bending with increasing the bending angle and less than 4.5% after bending for 1000 cycles with a bending angle of 180°. This indicates that strong conductive network of MWNTs coating on the nanofiber surface can not be destroyed even upon large strain. Therefore, such composite bundle can work well in the aspects that require severe bending such as electronic textiles. In addition, as shown in Figure 8c, the flexible composite nanofiber bundle can be easily tied into a knot without damaging the structure. Therefore, these MWNTs-adsorbed PA66 can be woven into textiles and show

DOI: 10.1021/acsami.6b02888
ACS Appl. Mater. Interfaces 2016, 8, 14150−14159

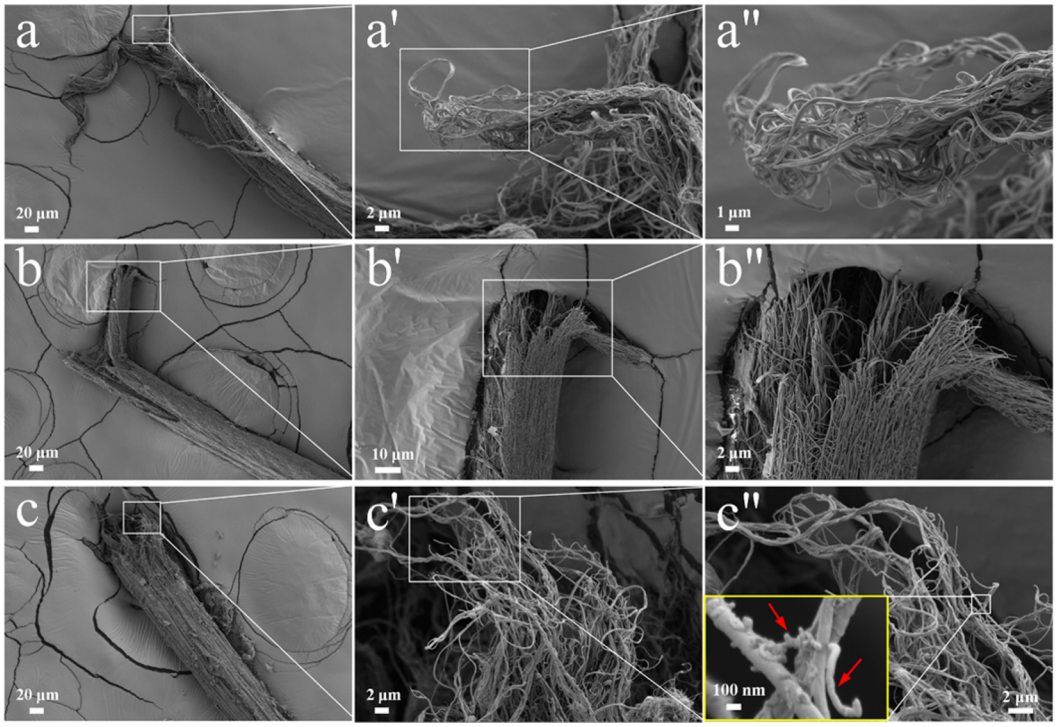

Figure 7. Tensile fracture surface of (a–a″) as-electrospun PA66, (b–b″) DMF-treated PA66, and (c–c″) MWNTs-adsorbed PA66 at different magnifications. The inset in (c″) is a higher magnification image from the fractured surface tip of MWNTs-adsorbed PA66.

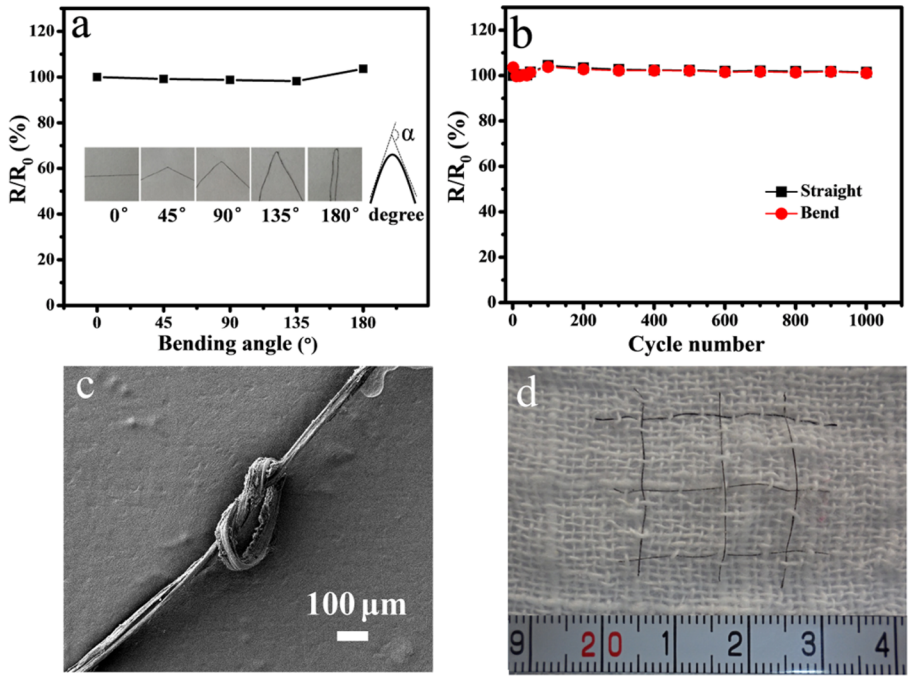

Figure 8. (a) Dependence of MWNTs-adsorbed PA66 bundle resistance on bent angle; (b) dependence of MWNTs-adsorbed PA66 bundle resistance on bent cycle number with a bent angle of 180°; (c) SEM image of a MWNTs-adsorbed PA66 nanofiber bundle being made into a knot; and (d) photograph of a cotton fabric incorporated with flexible MWNTs-adsorbed PA66 nanofiber bundles.

a promising potential for large-scale application, such as wearable and portable electronic devices,[10] flexible conductors for wearable electronic devices,[46] flexible electronic textiles, and fiber-shaped devices.[47] An optical photo of a cotton fabric incorporated with flexible MWNTs-adsorbed PA66 nanofiber bundles is shown in Figure 8d. These conductive composite bundles woven in the fabric are highly flexible. The above results indicate that such nanocomposite bundle has a high flexibility.

3.5. Temperature-Resistivity Behaviors. The potential use of MWNTs-adsorbed electrospun PA66 as temperature sensing materials was explored. Typical I–V curves for MWNTs-adsorbed PA66 at different temperatures are shown in Figure 9a. The resistance of MWNTs adsorbed PA66 is

DOI: 10.1021/acsami.6b02888
ACS Appl. Mater. Interfaces 2016, 8, 14150–14159

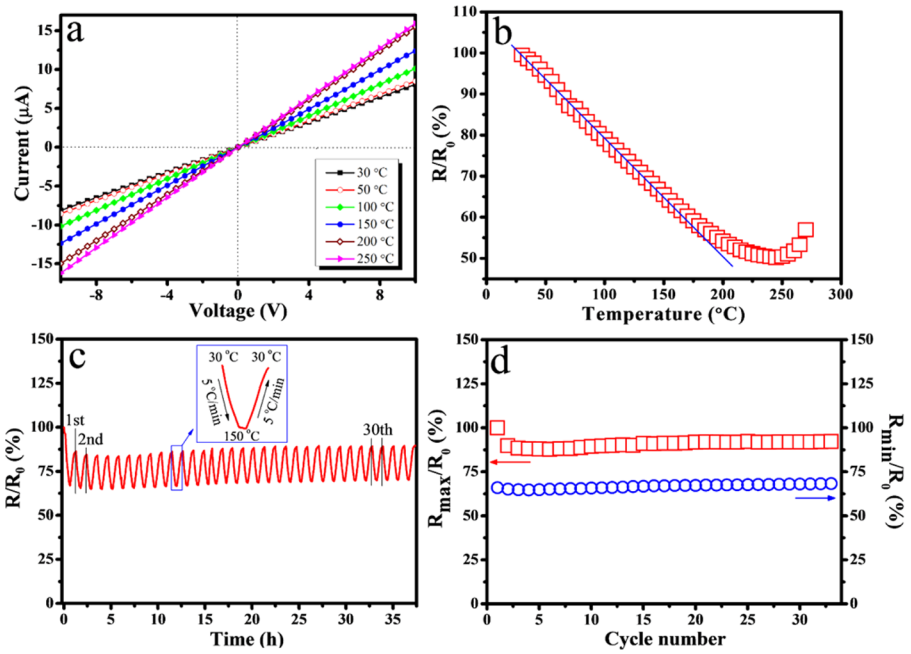

Figure 9. (a) Current−voltage characteristic curves of MWNTs-adsorbed PA66 at different temperatures; (b) resistance response of MWNTs-adsorbed PA66 from 30 to 270 °C; (c) resistance response of MWNTs-adsorbed PA66 vs temperature under repeated heating/cooling cycles (between 30 and 150 °C); and (d) relationships of R_{max}/R_0 and R_{min}/R_0 vs cycle number of MWNTs-adsorbed PA66.

observed to decrease with increasing the temperature at a given voltage. Moreover, these linear $I-V$ curves indicate ohmic behavior of the contacts between MWNTs-adsorbed PA66 and electrode, as well as ohmic conductivity of the MWNTs-adsorbed PA66 itself, demonstrating that such composite bundle can act as an ideal resistor in a wider temperature range.[48,49]

In order to observe the resistance response over a wide range of temperature, measurement was first carried out between 30 and 270 °C, Figure 9b. The recorded resistance values are normalized by the initial resistance values R_0 at 30 °C (viz., R/R_0). Generally, when the temperature is lower than 250 °C, the R/R_0 of MWNTs-adsorbed PA66 decreases with increasing the temperature, indicating that the MWNTs conductive network on PA66 nanofiber surface is improved with increasing the temperature. More importantly, from Figure 8b, the resistance/temperature dependence is observed to be close to linear if the applied temperature is lower than 150 °C, suggesting that the prepared MWNTs-adsorbed electrospun PA66 nanofiber bundles show application potentials as temperature sensors. With further increasing the temperature, the resistance decreases slowly and reaches the minimum at about 250 °C, indicating that the MWNTs adsorbed on nanofibers substantially contact each other. When temperature is above 250 °C, exceeding the melting point of MWNTs-adsorbed PA66 (see Figure S4), the R/R_0 dramatically increases because the bundle is melting and then fracture.

In order to further investigate the reversibility and repeatability of MWNTs-adsorbed PA66 as temperature sensors, the R/R_0 change of MWNTs-adsorbed PA66 during consecutive heating and cooling cycles was further conducted below 150 °C. The bundle was heated to 150 °C, and cooled down to 30 °C for 33 repeated cycles. Figure 9c shows the R/R_0 of MWNTs-adsorbed PA66 versus temperature. As shown in Figure 9c, MWNTs-adsorbed PA66 remains conductive after 33 consecutive cycles. In each cycle, the R/R_0 of the MWNTs-adsorbed PA66 first decreases sharply in a linear manner with increasing the temperature from 30 to 150 °C, followed by decreasing slightly when the temperature is hold at 150 °C, indicating that the adjustment of MWNTs conductive network is still ongoing when the temperature is constant, and then returns to a sharp increase in a linear manner during the process of cooling to 30 °C (see inset in Figure 9c). It is very interesting to observe that there is a linear dependence of the resistance on the applied temperature (inset in Figure 9c). More importantly, it can be seen that the curve of each cycle is identical with each other except for the first cycle. Figure 9d shows the relationships of R_{max}/R_0 and R_{min}/R_0 versus cycle number of MWNTs-adsorbed PA66, where R_{max} and R_{min} respectively represent the maximum and minimum value of resistance in each cycle. As shown in Figure 9d, the R_{max}/R_0 and R_{min}/R_0 have no obvious change from the second cycle. That is to say, except for the first cycle, when the applied temperature rises to 150 °C during each cycle, the resistance of the nanocomposite bundle decreases to an approximately fixed value. Then, if the applied temperature is decreased to 30 °C, the resistance returns to its initial value. This indicates that the resistance of MWNTs-adsorbed PA66 upon cyclic heating and cooling is highly reversible and reproducible when the temperature ranges from 30 to 150 °C. Due to the high conductivity, improved mechanical property, good flexibility, and linear temperature-resistance response, these MWNTs-adsorbed PA66 shows great potential as high temperature detector. Herein, we have fabricated a temperature detector by wrapping the MWNTs-adsorbed PA66 with a layer of polytetrafluoroethylene (PTFE) tape, followed by coating with a thin layer of silicon rubber (see Figure S5a). The measurement results after package (Figures S5b and S6) show that the MWNTs-adsorbed PA66 nanofiber bundles prepared in this study exhibit application potential as polymer-based flexible temperature sensors capable of working at high temperatures. More importantly, its highest working temper-

DOI: 10.1021/acsami.6b02888
ACS Appl. Mater. Interfaces 2016, 8, 14150−14159

ature of 150 °C is far exceeding that of other polymer-based temperature sensors reported recently.[50,51]

4. CONCLUSIONS

In summary, flexible and robust conductive nanocomposites of MWNTs-adsorbed PA66 nanofiber bundles were successfully manufactured through electrospinning and ultrasonication processing. The morphology and corresponding properties of the MWNTs-adsorbed PA66 composite nanofiber bundles were carefully investigated. The results show that MWNTs can be tightly adsorbed onto the electrospun PA66 nanofiber surface, simultaneously enhancing the electrical and mechanical properties of the electrospun PA66 nanofiber bundles. Moreover, the resistance of MWNTs-adsorbed PA66 composite nanofiber bundles has a linear dependence on the applied temperature as high as 150 °C. The highest working temperature of PA66 nanofiber bundle-based temperature sensor can reach as high as 150 °C, which is far exceeding that of other polymer-based temperature sensors reported previously. The results of this study indicate that MWNTs-adsorbed PA66 nanofiber bundles have great application potentials for temperature sensors, conductive textiles, wearable electronics, etc. Our work opens a new door toward fabricating flexible electronic devices with excellent mechanical property by using electrospun nanofibers.

■ ASSOCIATED CONTENT

Supporting Information

The Supporting Information is available free of charge on the ACS Publications website at DOI: 10.1021/acsami.6b02888.

Dependence of resistivity and conductivity on ultrasonication time with the same MWNT dispersion concentration of 0.05 wt % is shown in Figure S1, dependence of tensile strength and tensile fracture strain on ultrasonication time with the same MWNT dispersion concentration of 0.05 wt % is shown in Figure S2, the digital photo of the template used for mounting individual MWNTs-adsorbed PA66 nanofiber bundle for tensile test is shown in Figure S3, DSC curve of MWNTs-adsorbed PA66 nanofiber bundle (prepared with 0.05 wt % MWNT dispersion) in heating process is shown in Figure S4; digital photo of a temperature detector after package and a packaged temperature detector being wound onto a pin is shown in Figure S5; resistance response of the high-temperature sensor after being packaged with PTFE and silicon rubber under repeated heating/cooling cycles (between 30 and 150 °C) is shown in Figure S6 (PDF)

■ AUTHOR INFORMATION

Corresponding Authors

*E-mail: gqzheng@zzu.edu.cn (G.Z.).
*E-mail: shency@zzu.edu.cn (C.S.).
*E-mail: zguo10@utk.edu (Z.G.).

Notes

The authors declare no competing financial interest.

■ ACKNOWLEDGMENTS

This project is financially supported by the National Natural Science Foundation of China (11432003, 11572290), the Major State Basic Research Projects (2012CB025904), HASTIT, and Plan for Scientific Innovation Talent of Henan Province for financial support. Z.G. appreciates the start-up funds from University of Tennessee.

■ REFERENCES

(1) Doshi, J.; Reneker, D. H. Electrospinning Process and Applications of Electrospun Fibers. *J. Electrost.* **1995**, *35* (2−3), 151−160.
(2) Xia, Y.; Yang, P.; Sun, Y.; Wu, Y.; Mayers, B.; Gates, B.; Yin, Y.; Kim, F.; Yan, H. One-Dimensional Nanostructures: Synthesis, Characterization, and Applications. *Adv. Mater.* **2003**, *15* (5), 353−389.
(3) Huang, Z.-M.; Zhang, Y. Z.; Kotaki, M.; Ramakrishna, S. A Review on Polymer Nanofibers by Electrospinning and Their Applications in Nanocomposites. *Compos. Sci. Technol.* **2003**, *63* (15), 2223−2253.
(4) Li, D.; Xia, Y. Electrospinning of Nanofibers: Reinventing the Wheel? *Adv. Mater.* **2004**, *16* (14), 1151−1170.
(5) Smit, E.; Bűttner, U.; Sanderson, R. D. Continuous Yarns from Electrospun Fibers. *Polymer* **2005**, *46* (8), 2419−2423.
(6) Wu, S.; Wang, B.; Zheng, G.; Liu, S.; Dai, K.; Liu, C.; Shen, C. Preparation and Characterization of Macroscopically Electrospun Polyamide 66 Nanofiber Bundles. *Mater. Lett.* **2014**, *124*, 77−80.
(7) Jana, S.; Cooper, A.; Ohuchi, F.; Zhang, M. Uniaxially Aligned Nanofibrous Cylinders by Electrospinning. *ACS Appl. Mater. Interfaces* **2012**, *4* (9), 4817−4824.
(8) Liang, Y.; Liu, S.; Dai, K.; Wang, B.; Shao, C.; Zhang, Q.; Wang, S.; Zheng, G.; Liu, C.; Chen, J.; Shen, C.; Li, Q.; Peng, X. Transcrystallization in Nanofiber Bundle/Isotactic Polypropylene Composites: Effect of Matrix Molecular Weight. *Colloid Polym. Sci.* **2012**, *290* (12), 1157−1164.
(9) Lee, J.; Deng, Y. Increased Mechanical Properties of Aligned and Isotropic Electrospun PVA Nanofiber Webs by Cellulose Nanowhisker Reinforcement. *Macromol. Res.* **2012**, *20* (1), 76−83.
(10) Chen, X.; Lin, H.; Deng, J.; Zhang, Y.; Sun, X.; Chen, P.; Fang, X.; Zhang, Z.; Guan, G.; Peng, H. Electrochromic Fiber-Shaped Supercapacitors. *Adv. Mater.* **2014**, *26* (48), 8126−8132.
(11) Zhou, F.-L.; Gong, R.-H. Manufacturing Technologies of Polymeric Nanofibres and Nanofibre Yarns. *Polym. Int.* **2008**, *57* (6), 837−845.
(12) Xu, Y.; Wu, J.; Wang, H.; Li, H.; Di, N.; Song, L.; Li, S.; Li, D.; Xiang, Y.; Liu, W.; Mo, X.; Zhou, Q. Fabrication of Electrospun Poly(l-Lactide-co-E-Caprolactone)/Collagen Nanoyarn Network as a Novel, Three-dimensional, Macroporous, Aligned Scaffold for Tendon Tissue Engineering. *Tissue Eng., Part C* **2013**, *19* (12), 925−936.
(13) Pierre-Alexis, M.; Nasim, Z.; Osnat, H.; Emilie, L.; Andrew, C. Fabrication of Continuous Electrospun Filaments with Potential for Use as Medical Fibres. *Biofabrication* **2015**, *7* (2), 025006.
(14) Wu, S.; Zheng, G.; Guan, X.; Yan, X.; Guo, J.; Dai, K.; Liu, C.; Shen, C.; Guo, Z. Mechanically Strengthened Polyamide 66 Nanofibers Bundles via Compositing With Polyvinyl Alcohol. *Macromol. Mater. Eng.* **2016**, *301* (2), 212−219.
(15) Niu, H.; Gao, W.; Lin, T.; Wang, X.; Kong, L. Composite Yarns Fabricated From Continuous Needleless Electrospun Nanofibers. *Polym. Eng. Sci.* **2014**, *54* (7), 1495−1502.
(16) Barani, H. Antibacterial Continuous Nanofibrous Hybrid Yarn Through In Situ Synthesis of Silver Nanoparticles: Preparation and Characterization. *Mater. Sci. Eng., C* **2014**, *43*, 50−57.
(17) Baniasadi, M.; Huang, J.; Xu, Z.; Moreno, S.; Yang, X.; Chang, J.; Quevedo-Lopez, M. A.; Naraghi, M.; Minary-Jolandan, M. High-Performance Coils and Yarns of Polymeric Piezoelectric Nanofibers. *ACS Appl. Mater. Interfaces* **2015**, *7* (9), 5358−5366.
(18) Lin, D.-P.; He, H.-W.; Huang, Y.-Y.; Han, W.-P.; Yu, G.-F.; Yan, X.; Long, Y.-Z.; Xia, L.-H. Twisted Microropes for Stretchable Devices Based on Electrospun Conducting Polymer Fibers Doped with Ionic Liquid. *J. Mater. Chem. C* **2014**, *2* (42), 8962−8966.
(19) Fong, H.; Liu, W.; Wang, C.-S.; Vaia, R. A. Generation of Electrospun Fibers of Nylon 6 and Nylon 6-Montmorillonite Nanocomposite. *Polymer* **2002**, *43* (3), 775−780.

DOI: 10.1021/acsami.6b02888
ACS Appl. Mater. Interfaces 2016, 8, 14150−14159

(20) Teo, W. E.; Ramakrishna, S. Electrospun Fibre Bundle Made of Aligned Nanofibres over Two Fixed Points. *Nanotechnology* **2005**, *16* (9), 1878−1884.
(21) Jalili, R.; Morshed, M.; Abdolkarim, S.; Ravandi, H. Fundamental Parameters Affecting Electrospinning of PAN Nanofibers as Uniaxially Aligned Fibers. *J. Appl. Polym. Sci.* **2006**, *101* (6), 4350−4357.
(22) Afifi, A. M.; Nakajima, H.; Yamane, H.; Kimura, Y.; Nakano, S. Fabrication of Aligned Poly(L-lactide) Fibers by Electrospinning and Drawing. *Macromol. Mater. Eng.* **2009**, *294* (10), 658−665.
(23) Maheshwari, S.; Chang, H.-C. Assembly of Multi-Stranded Nanofiber Threads through AC Electrospinning. *Adv. Mater.* **2009**, *21* (3), 349−354.
(24) Wang, X.; Zhang, K.; Zhu, M.; Hsiao, B. S.; Chu, B. Enhanced Mechanical Performance of Self-Bundled Electrospun Fiber Yarns via Post-Treatments. *Macromol. Rapid Commun.* **2008**, *29* (10), 826−831.
(25) Barber, J. G.; Handorf, A. M.; Allee, T. J.; Li, W.-J. Braided Nanofibrous Scaffold for Tendon and Ligament Tissue Engineering. *Tissue Eng., Part A* **2013**, *19* (11−12), 1265−1274.
(26) Shaffer, M. S. P.; Windle, A. H. Fabrication and Characterization of Carbon Nanotube/Poly(vinyl alcohol) Composites. *Adv. Mater.* **1999**, *11* (11), 937−941.
(27) Qian, D.; Dickey, E. C.; Andrews, R.; Rantell, T. Load Transfer and Deformation Mechanisms in Carbon Nanotube-Polystyrene Composites. *Appl. Phys. Lett.* **2000**, *76* (20), 286810.1063/1.126500.
(28) Zhang, W. D.; Shen, L.; Phang, I. Y.; Liu, T. Carbon Nanotubes Reinforced Nylon-6 Composite Prepared by Simple Melt-Compounding. *Macromolecules* **2004**, *37* (2), 256−259.
(29) Pötschke, P.; Fornes, T. D.; Paul, D. R. Rheological Behavior of Multiwalled Carbon Nanotube/Polycarbonate Composites. *Polymer* **2002**, *43* (11), 3247−3255.
(30) Vigolo, B.; Pénicaud, A.; Coulon, C.; Sauder, C.; Pailler, R.; Journet, C.; Bernier, P.; Poulin, P. Macroscopic Fibers and Ribbons of Oriented Carbon Nanotubes. *Science* **2000**, *290* (5495), 1331−1334.
(31) Vigolo, B.; Poulin, P.; Lucas, M.; Launois, P.; Bernier, P. Improved Structure and Properties of Single-Wall Carbon Nanotube Spun Fibers. *Appl. Phys. Lett.* **2002**, *81* (7), 1210−1212.
(32) Kumar, S.; Dang, T. D.; Arnold, F. E.; Bhattacharyya, A. R.; Min, B. G.; Zhang, X.; Vaia, R. A.; Park, C.; Adams, W. W.; Hauge, R. H.; Smalley, R. E.; Ramesh, S.; Willis, P. A. Synthesis, Structure, and Properties of PBO/SWNT Composites. *Macromolecules* **2002**, *35* (24), 9039−9043.
(33) Baughman, R. H.; Zakhidov, A. A.; de Heer, W. A. Carbon Nanotubes–the Route Toward Applications. *Science* **2002**, *297* (5582), 787−792.
(34) Coleman, J. N.; Khan, U.; Blau, W. J.; Gun'ko, Y. K. Small but Strong: A Review of the Mechanical Properties of Carbon Nanotube−Polymer Composites. *Carbon* **2006**, *44* (9), 1624−1652.
(35) Abbasipour, M.; Khajavi, R. Nanofiber Bundles and Yarns Production by Electrospinning: A Review. *Adv. Polym. Technol.* **2013**, *32* (3), 21363.
(36) Ko, F.; Gogotsi, Y.; Ali, A.; Naguib, N.; Ye, H.; Yang, G. L.; Li, C.; Willis, P. Electrospinning of Continuous Carbon Nanotube-Filled Nanofiber Yarns. *Adv. Mater.* **2003**, *15* (14), 1161−1165.
(37) Uddin, N. M.; Ko, F.; Xiong, J.; Farouk, B.; Capaldi, F. Process, Structure, and Properties of Electrospun Carbon Nanotube-Reinforced Nanocomposite Yarns. *Res. Lett. Mater. Sci.* **2009**, *2009*, 5.
(38) Kim, H. S.; Jin, H.-J.; Myung, S. J.; Kang, M.; Chin, I.-J. Carbon Nanotube-Adsorbed Electrospun Nanofibrous Membranes of Nylon 6. *Macromol. Rapid Commun.* **2006**, *27* (2), 146−151.
(39) Wei, Z.; Peng, M.; Qiu, F.; Wang, X.; Shengru, l.; Yang, J. Development of a Novel Preparation Method for Conductive PES Ultrafine Fibers with Self-Formed Thin PES/CNTs Composite Layer by Vapor Treatment. *RSC Adv.* **2015**, *5* (53), 42305−42310.
(40) Berber, S.; Kwon, Y.-K.; Tománek, D. Unusually High Thermal Conductivity of Carbon Nanotubes. *Phys. Rev. Lett.* **2000**, *84* (20), 4613−4616.
(41) Choi, J.; Park, D.; Shim, S. Chemical Vapour Sensing Behaviors of Multi-Walled Carbon Nanotube Adsorbed Electrospun Nylon 6,6 Nanofibers. *Macromol. Res.* **2011**, *19* (9), 980−983.
(42) Gao, J.; Li, W.; Shi, H.; Hu, M.; Li, R. K. Y. Preparation, Morphology, and Mechanical Properties of Carbon Nanotube Anchored Polymer Nanofiber Composite. *Compos. Sci. Technol.* **2014**, *92*, 95−102.
(43) Lu, B.; Zheng, G.; Dai, K.; Liu, C.; Chen, J.; Shen, C. Enhanced Mechanical Properties of Polyethylene Composites with Low Content of Electrospun Nylon-66 Nanofibers. *Mater. Lett.* **2015**, *140*, 131−134.
(44) Mercante, L. A.; Pavinatto, A.; Iwaki, L. E. O.; Scagion, V. P.; Zucolotto, V.; Oliveira, O. N.; Mattoso, L. H. C.; Correa, D. S. Electrospun Polyamide 6/Poly(allylamine hydrochloride) Nanofibers Functionalized with Carbon Nanotubes for Electrochemical Detection of Dopamine. *ACS Appl. Mater. Interfaces* **2015**, *7* (8), 4784−4790.
(45) Vankayala, R. R.; Lai, W.-J. P.; Cheng, K.-C.; Hwang, K. C. Enhanced Electrical Conductivity of Nylon 6 Composite Using Polyaniline-Coated Multi-Walled Carbon Nanotubes as Additives. *Polymer* **2011**, *52* (15), 3337−3343.
(46) Peng, H.; Jain, M.; Li, Q.; Peterson, D. E.; Zhu, Y.; Jia, Q. Vertically Aligned Pearl-like Carbon Nanotube Arrays for Fiber Spinning. *J. Am. Chem. Soc.* **2008**, *130* (4), 1130−1131.
(47) Zhang, Z.; Li, X.; Guan, G.; Pan, S.; Zhu, Z.; Ren, D.; Peng, H. A Lightweight Polymer Solar Cell Textile that Functions when Illuminated from Either Side. *Angew. Chem., Int. Ed.* **2014**, *53* (43), 11571−11574.
(48) Dorozhkin, P. S.; Tovstonog, S. V.; Golberg, D.; Zhan, J.; Ishikawa, Y.; Shiozawa, M.; Nakanishi, H.; Nakata, K.; Bando, Y. A Liquid-Ga-Filled Carbon Nanotube: A Miniaturized Temperature Sensor and Electrical Switch. *Small* **2005**, *1* (11), 1088−1093.
(49) Mahanandia, P.; Singh, L. T.; Nanda, K. K. Possible Application of Carbon Nanotube Bundles for Low Temperature Sensing. *Rev. Sci. Instrum.* **2008**, *79* (5), 053909.
(50) Blasdel, N. J.; Wujcik, E. K.; Carletta, J. E.; Lee, K. S.; Monty, C. N. Fabric Nanocomposite Resistance Temperature Detector. *IEEE Sens. J.* **2015**, *15* (1), 300−306.
(51) Sadasivuni, K. K.; Kafy, A.; Kim, H.-C.; Ko, H.-U.; Mun, S.; Kim, J. Reduced Graphene Oxide Filled Cellulose Films for Flexible Temperature Sensor Application. *Synth. Met.* **2015**, *206*, 154−161.

DOI: 10.1021/acsami.6b02888
ACS Appl. Mater. Interfaces 2016, 8, 14150−14159